arXiv:1609.06697v1 [stat.ME] 21 Sep 2016

On the estimation of parameters of a spheroid distribution from planar sections

Markus Baaske[1], Felix Ballani[1], and Alexandra Illgen[2]

[1]Institute of Stochastics, Technische Universität Bergakademie Freiberg, D-09596 Freiberg, Germany

[2]Institute of Materials Engineering, Technische Universität Bergakademie Freiberg, D-09596 Freiberg, Germany

September 22, 2016

Abstract

We study two different methods for inferring the parameters of a spheroid distribution from planar sections of a stationary spatial system of spheroids: one method first unfolds non-parametrically the joint size-shape-orientation distribution related to the observable ellipses in the plane into the joint size-shape-orientation distribution related to the spheroids followed by a maximum likelihood estimation of the parameters; the second method directly estimates these parameters based on statistics of the observable ellipses using a quasi-likelihood approach. As an application we consider two metal matrix composites with ceramic particles and, respectively, short fibres as reinforcing inclusions, model both types of inclusions as prolate spheroids and estimate the parameters of their distribution from planar sections.

MSC 2010 Classification: Primary: 62F10, 62M30; Secondary: 60D05, 60G10, 60G55

Keywords: Spheroid distribution; Trivariate unfolding; Quasi-likelihood estimation; Stereology

1 Introduction

Although nowadays several imaging techniques like X-ray computed tomography are available by which means a three-dimensional specimen, e. g. a composite material, can be represented truly three-dimensional for further analysis this is sometimes too expensive or not applicable due to the type of material, or, the resolution of the sampling technique is too low in order to distinguish very small substructures or inclusions. However, the geometry of such spatial structures still allows for investigation via planar sections where then often more highly resolving sampling techniques are available (Nagel, 2010). The methodology aimed to draw inference from information contained in planar sections about the spatial geometrical structure is part of stereology (Ohser and Mücklich, 2000; Nagel, 2010; Chiu et al., 2013).

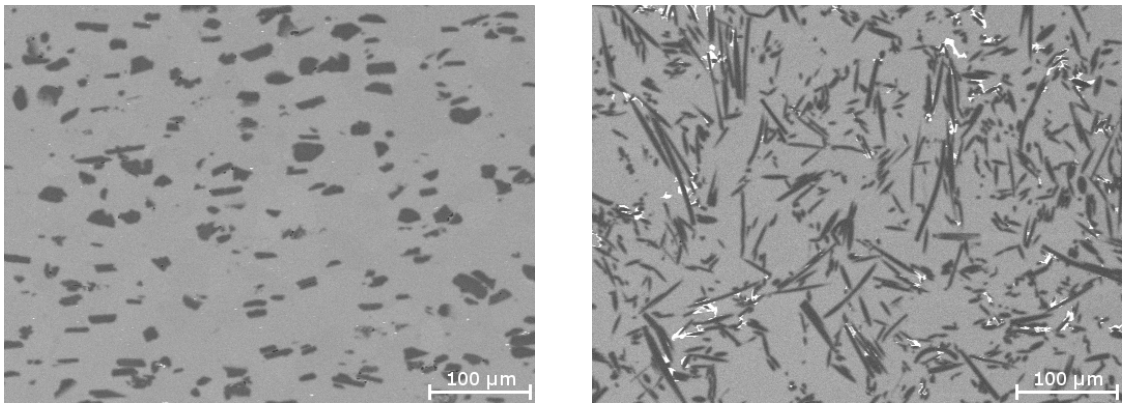

Figure 1: Planar sections (cutout) of metal matrix composites with reinforcing ceramic particles (left) and short fibres (right) resulting from scanning electron microscopy.

We were faced with this kind of situation when investigating and modelling metal-matrix composites with either ceramic particles or short ceramic fibres as reinforcing inclusions (see Figure 1) with respect to their fatigue behaviour. The kind of model intended for the fatigue behaviour (discussed elsewhere) is based on a model for the spatial configuration of the ceramic inclusions. Besides a model for the spatial arrangement of the inclusions (also discussed elsewhere) we were interested in a model for the distribution of the inclusions in the sense of a random compact set. Under the assumption of spatial stationarity it is justified to speak of the typical inclusion whose distribution does not depend on the particular (stationary) spatial arrangement of the inclusions (cf. e. g. Schneider and Weil, 2008, Sect. 4.2). With this reasoning in mind and since in the present paper we solely focus on the distribution of the typical inclusion we will throughout the paper work with a stationary *Poisson* particle process (Schneider and Weil, 2008, Sect. 4.1) for the spatial arrangement even when processing the data (where the Poisson assumption is certainly not true).

In particular due to the possible flexibility w.r.t. shape we decided to model the typical inclusion as a random *ellipsoid* with randomness in size, shape and orientation. Thus it is then natural to model the intersected inclusions in the observable planar sections as *ellipses* for which size, shape and orientation (in the plane) can be estimated from digital images.

Dating back to Wicksell (1926) the respective stereological objective is to infer the joint distribution of the ellipsoids' size and shape (and later also orientation) from the ellipses observable in the planar section which turned out to be solvable completely and uniquely only in case the ellipsoids are all either prolate or oblate spheroids (ellipsoids of revolution), see Cruz-Orive (1976). The corresponding solution of unfolding the joint size-shape-orientation distribution related to the observable ellipses in the plane into the joint size-shape-orientation distribution related to the spheroids was given by Beneš et al. (1997) and Beneš and Krejčíř (1997), see also Beneš and Rataj (2004, Ch. 6). Hence, from the empirical unfolded joint size-shape-orientation distribution, typically available as a histogram, one may estimate the parameters of a parametric spheroid distribution, for instance by the maximum likelihood method.

A different way is to estimate the parameters based on statistics directly available from the joint size-shape-orientation distribution related to the ellipses. A general approach for such

a kind of estimation would be to find those model parameters which lead to statistics most similar to the observed ones in the sense of a least squares or minimum contrast approach. Instead of minimizing a distance a related alternative is to find the root of an estimation equation. A particular such estimation equation is based on the so-called quasi-score function which leads to quasi-likelihood estimation, see Heyde (1997) for the general theory. A general problem which holds both for finding a minimum or a root is to explore efficiently the space of possible parameters in case the objective function can be determined only by simulations. For quasi-likelihood estimation an approach is given in Baaske et al. (2014).

Our idea to compare the (possibly more established) way of estimating the parameters by the maximum likelihood method based on the stereologically unfolded joint size-shape-orientation distribution with the quasi-likelihood estimation approach is motivated by the following facts. On the one hand, quasi-likelihood estimation based on simulations is much more involved than unfolding followed by maximum likelihood estimation. On the other hand, unfolding as the solution of an ill-posed inverse problem has a tendency to corrupt the subsequent parameter estimation whereas in quasi-likelihood estimation the available information contained in the employed statistics is used in an optimal way, the latter being demonstrated in Baaske et al. (2014) with an example in a spatial context, leading to comparatively more precise estimation results.

The paper is organized as follows. In Section 2 we introduce the parametric model for a spheroid distribution for which we aim to estimate parameters. Furthermore, in Section 3, we first summarize the necessary facts for the trivariate unfolding related to prolate spheroids and give then details for the subsequent maximum likelihood estimation. In Section 4 we sketch the ideas of the quasi-likelihood estimation approach. Then, in Section 5, we compare both approaches by means of a simulation study. Finally, in Section 6 we apply them to planar sections of a system of particles and a system of short fibres, and end up with some conclusions in Section 7.

2 A parametric spheroid distribution

Since the stereological unfolding of the joint size-shape-orientation distribution of a population of ellipsoids from corresponding ellipses observable in a planar section is reasonable solvable only in case the ellipsoids are all either prolate or oblate spheroids (Cruz-Orive, 1976) and in view of the short fibres in our application we restrict henceforth to *prolate* spheroids with lengths $a \geq b = c$ of the semi-axes. The shape factor s of such a prolate spheroid is then defined as $s = c/a$ and satisfies $0 < s \leq 1$. Finally, the orientation of a prolate spheroid as the direction of the axis of revolution can be described in terms of spherical coordinates (ϑ, φ) w.r.t. a fixed axis u with polar angle $\vartheta \in [0, \pi/2)$ and azimuthal angle $\varphi \in [0, 2\pi)$. Hence, besides location, a (prolate) spheroid is described for instance by $(a, s, \vartheta, \varphi)$ or $(c, s, \vartheta, \varphi)$, respectively

To simplify matter we assume that the distribution of the orientations is independent of that of the sizes and shapes. Furthermore, the production process justifies the assumption that the distribution of the system of spheroids is invariant w.r.t. rotations about the fixed axis u. One such model for the random orientation of a spheroid respecting this kind of invariance is the 'Schladitz distribution' (Franke et al., 2016) which has probability density function (p.d.f.)

$$h_\beta(\vartheta, \varphi) = \frac{1}{2\pi} \cdot \frac{1}{2} \frac{\beta \sin \vartheta}{(1 + (\beta^2 - 1)\cos^2 \vartheta)^{\frac{3}{2}}}, \quad \vartheta \in [0, \pi), \varphi \in [0, 2\pi), \tag{1}$$

see also Ohser and Schladitz (2009, Eq. (7.11)). In this model $\beta > 0$ is an anisotropy parameter in the sense that for decreasing $\beta < 1$ the spheroids tend to be more and more parallel to the u-axis, and, respectively, for increasing $\beta > 1$ the spheroids tend to be more and more parallel to the plane perpendicular to u, and $\beta = 1$ is the case of isotropically distributed directions.

Since in particular the population of particles suggests a possible dependence of size and shape of the modelling ellipsoids and a typical size distribution for granular inclusions in materials science is the log-normal distribution we aim to work with the following model for the length a of the semi-major axis and the shape s. Let (ξ, η) be a bivariate normally distributed random vector with mean vector $\mu = (\mu_1, \mu_2) \in \mathbb{R}^2$ and variance-covariance-matrix

$$\Sigma = \begin{pmatrix} \sigma_1^2 & \varrho\sigma_1\sigma_2 \\ \varrho\sigma_1\sigma_2 & \sigma_2^2 \end{pmatrix}, \quad \sigma_1, \sigma_2 \geq 0, -1 \leq \varrho \leq 1. \tag{2}$$

Then let

$$a = \exp(\xi), \quad s = \frac{1}{1 + \exp(-\eta)}. \tag{3}$$

Hence, a and s are independent if and only if $\varrho = 0$. Furthermore, for $\sigma_1 = 0$ or $\sigma_2 = 0$ the cases of a deterministic size or a deterministic shape are included.

All in all we end up with a parametric model for the size-shape-orientation distribution of a random spheroid including the six parameters $(\mu_1, \mu_2, \sigma_1, \sigma_2, \varrho, \beta)$. If a system of n spheroids (for instance associated with the ceramic inclusions) was observable directly in terms of (a_l, s_l, ϑ_l), $l = 1, \ldots, n$, then the usual way of parameter estimation would be the maximum likelihood method since the likelihood is available. In what follows we discuss two ways how the model parameters might be estimated in case only planar sections of the inclusions are given.

3 Maximum likelihood estimation after trivariate unfolding

3.1 Unfolding

Let Ψ_V be a stationary spheroid process with intensity λ_V which is intersected by a random plane $\mathcal{H}$ with normal direction v perpendicular to the reference direction u, i. e. v has polar angle $\pi/2$ and uniformly on $[0, 2\pi)$ distributed azimuthal angle w.r.t. u (termed 'vertical uniform random section' in case $u = (0, 0, 1)$, see Beneš and Rataj, 2004). In case a spheroid is hit by $\mathcal{H}$ the intersection of both is an ellipse with lengths A and C, $A \geq C$, of the two semi-axes, related shape factor $S = C/A$ and angle α between the semi-major axis and the reference direction u. The cumulative distribution function (c.d.f.) $G(C, S, \alpha)$ of the triple (C, S, α) related to the typical intersection ellipse and the c.d.f. $H(c, s, \vartheta)$ of the triple (c, s, ϑ) related to the typical spheroid are related to each other by the integral equation

$$\lambda_A G(C, S, \alpha) = \frac{4}{\pi}\lambda_V \int \mathbf{1}_{[C,\infty)}(c)(c - \sqrt{c^2 - C^2})K_0(\alpha, S, \vartheta, s)\,\mathrm{d}H(c, s, \vartheta), \tag{4}$$

see Beneš and Rataj (2004, Thm. 6.17), where λ_A is the intensity of the stationary intersection ellipse process and $K_0(\alpha, S, \vartheta, s)$ is some function, the explicit form of which is omitted here and can be found in the cited theorem. Based on the observations (C_l, S_l, α_l), $l = 1, \ldots, n$, the objective of unfolding is to reconstruct $H(c, s, \vartheta)$ by solving (4) for $H(c, s, \vartheta)$. The numerical solution presented in Beneš and Rataj (2004, Sect. 6.3.3), which we aim to apply in what

follows, transforms the integral equation (4) into a system of linear equations by discretization and solves this system with the help of the expectation-maximization algorithm. The discretization is based on classes

$$D_{ijk} = \{(c, s, \vartheta) : c_{i-1} < c \leq c_i, s_{j-1} < s \leq s_j, \vartheta_{k-1} < \vartheta \leq \vartheta_k\},$$

$i = 1, \ldots, N_c$, $j = 1, \ldots, N_s$, $k = 1, \ldots, N_\vartheta$, and, respectively,

$$\tilde{D}_{IJK} = \{(C, S, \alpha) : C_{I-1} < C \leq C_I, S_{J-1} < S \leq S_J, \alpha_{K-1} < \alpha \leq \alpha_K\},$$

$I = 1, \ldots, N_C$, $J = 1, \ldots, N_S$, $K = 1, \ldots, N_\alpha$, where for simplicity we work with $N_C = N_c$, $N_S = N_s$, $N_\alpha = N_\vartheta$ and $\tilde{D}_{ijk} = D_{ijk}$ for all (i, j, k).

From the planar observations first a normalized trivariate histogram with relative frequencies g_{ijk} related to class D_{ijk} is determined. Then unfolding results in another normalized trivariate histogram with relative frequencies h_{ijk} which is a kind of kernel density estimation of the probability density function of $H(c, s, \vartheta)$.

The whole unfolding procedure as in Beneš and Rataj (2004, Sect. 6.3.3) adapted to the case of prolate spheroids is available within the contributed R-package unfoldr, see Baaske (2016a).

3.2 Maximum likelihood estimation

Since the result of the unfolding is the trivariate size-shape-orientation histogram (h_{ijk}) a subsequent maximum likelihood estimation has to based on that and not on the original likelihood related to (c, s, ϑ) or, equivalently, (a, s, ϑ).

In the model introduced in Section 2 we assume that the orientation of the spheroids is independent of size and shape. Hence the parameter β of the orientation distribution can be estimated separately. The respective log-likelihood reads

$$\log\left(L\left((h_{..k}); \beta\right)\right) = \sum_{k=1}^{N_\vartheta} h_{..k} \log\left(\mathrm{P}_\beta\big((\vartheta_{k-1}, \vartheta_k]\big)\right)$$

where P_β denotes the probability measure related to the p.d.f. h_β,

$$h_{..k} = \sum_{i=1}^{N_c} \sum_{j=1}^{N_s} h_{ijk}$$

is the marginal relative frequency in bin $(\vartheta_{k-1}, \vartheta_k]$, $k = 1, \ldots, N_\vartheta$, and N_c, N_s and N_ϑ are the numbers of bins for, respectively, c, s and ϑ as in Section 3.1.

Furthermore, with $f_{\mu,\Sigma}$ the p.d.f. of a bivariate normal distribution with mean $\mu = (\mu_1, \mu_2)$ and variance-covariance matrix Σ as in (2), the joint p.d.f. of the length c of the semi-minor axis and the shape factor s is

$$h_{\mu,\Sigma}(c, s) = \frac{1}{c\, s\, (1 - s)}\, f_{\mu,\Sigma}(\log(c/s), \log(s/(1 - s)))$$

since the reverse transform of $(\xi, \eta) \mapsto (c, s) = (\exp(\xi)/(1 + \exp(-\eta)), 1/(1 + \exp(-\eta)))$ as in (3) is $(c, s) \mapsto (\xi, \eta) = (\log(c/s), \log(s/(1 - s)))$ with Jacobian $(c\, s\, (1 - s))^{-1}$. Then, denoting

by $\mathrm{P}_{\mu,\Sigma}$ the probability measure related to the p.d.f. $h_{\mu,\Sigma}$, the log-likelihood reads

$$\log\left(L\left((h_{ij\cdot});\mu,\Sigma\right)\right)=\sum_{i=1}^{N_c}\sum_{j=1}^{N_s}h_{ij\cdot}\log\left(\mathrm{P}_{\mu,\Sigma}\big((c_{i-1},c_i]\times(s_{j-1},s_j]\big)\right),$$

where

$$h_{ij\cdot}=\sum_{k=1}^{N_\vartheta}h_{ijk}$$

is the marginal relative frequency in the class $(c_{i-1},c_i]\times(s_{j-1},s_j]$, $i=1,\ldots,N_s$, $j=1,\ldots,N_c$.

4 Quasi-likelihood estimation

The idea of the quasi-likelihood estimation approach which we aim to apply is to estimate the unknown parameter θ (taking values in an open subset Θ of the q-dimensional Euclidean space $\mathbb{R}^q$) by finding a root $\hat{\theta}_{QL}$ of the quasi-score estimating function

$$Q(\theta,y)=\left(\frac{\partial\mathsf{E}_\theta(T(X))}{\partial\theta}\right)^\top\mathsf{Var}_\theta(T(X))^{-1}(y-\mathsf{E}_\theta(T(X))),\tag{5}$$

where X is a random variable on the sample space $\mathbb{X}$ with distribution P_θ, $T\colon\mathbb{X}\to\mathbb{R}^p$ is a transformation of X to a set of summary statistics, $y=T(x)$ is the respective (column) vector of summary statistics for the observed data x, $\top$ denotes transpose, and, respectively, E_θ and Var_θ denote expectation and variance w.r.t. P_θ. For a fixed set of summary statistics T, the quasi-score estimating function Q in (5) is that standardized estimation function

$$\tilde{G}=-\left(\mathsf{E}_\theta\left[\frac{\partial G}{\partial\theta}\right]\right)^\top\left(\mathsf{E}_\theta\left[GG^\top\right]\right)^{-1}G\tag{6}$$

for which the information criterion

$$\mathcal{E}(G)=\mathsf{E}_\theta(\tilde{G}\tilde{G}^\top)=\left(\mathsf{E}_\theta\left[\frac{\partial G}{\partial\theta}\right]\right)^\top\left(\mathsf{E}_\theta\left[GG^\top\right]\right)^{-1}\left(\mathsf{E}_\theta\left[\frac{\partial G}{\partial\theta}\right]\right)\tag{7}$$

is maximized in the partial order of non-negative definite matrices (Heyde, 1997) among all *linear* unbiased estimating functions $G(\theta,y)=A(\theta)(y-\mathsf{E}_\theta(T(X)))$, where $A(\theta)$ is any non-singular matrix.

The information criterion in (7) is a generalization of the well-known Fisher information since it coincides with the Fisher information in case a likelihood is available and G equals the usual score function. Then, in analogy to maximum likelihood estimation, the inverse of $\mathcal{E}(G)$ has a direct interpretation as the asymptotic variance of the estimator $\hat{\theta}_{QL}$. For the quasi-likelihood estimation based on (5) and the particular vector T of summary statistics the information criterion reads

$$I_T(\theta)=\mathsf{Var}_\theta(Q(\theta,T(X)))=\left(\frac{\partial\mathsf{E}_\theta(T(X))}{\partial\theta}\right)^\top\mathsf{Var}_\theta(T(X))^{-1}\left(\frac{\partial\mathsf{E}_\theta(T(X))}{\partial\theta}\right)\tag{8}$$

and is called *quasi-information matrix* in what follows.

Similar to finding a root of the score in maximum likelihood estimation by Fisher scoring, the quasi-score equation (5) can be solved with the *Fisher quasi-scoring iteration*

$$\theta^{(k+1)} = \theta^{(k)} + t^{(k)}\delta^{(k)}, \quad \delta^{(k)} = I_T(\theta^{(k)})^{-1}Q(\theta^{(k)}, y), \tag{9}$$

where $t^{(k)}$ is some step length parameter (Osborne, 1992; Baaske et al., 2014), in case the quasi-score Q and the quasi-information matrix I_T are available as a closed form expression which can be evaluated at least numerically. In particular, this would include to know expectations and variances of the employed summary statistics T w.r.t. to P_θ as a function of θ. However, in many cases including the setting under investigation these expectations and variances are available only as Monte Carlo estimates based on simulated realizations of the random variable X under P_θ. Then, still, (9) might be applied in case simulations are fast and thus the Monte Carlo error can be made small by a sufficiently large number of used model realizations. For more involved simulations, however, a Monte Carlo error cannot be avoided, making a direct application of (9) unreasonable. In Baaske et al. (2014) an idea is presented how the quasi-likelihood estimation approach can be applied even in that case. A respective routine has been developed within the contributed R-package QLE (Baaske, 2016b).

5 Simulation study

The generation of the data for the simulation study includes the following steps. First a realization of a stationary Poisson spheroid process with some fixed intensity λ_V and with distribution P_θ, $\theta = (\mu_1, \mu_2, \sigma_1, \sigma_2, \varrho, \beta)$, related to the typical (prolate) spheroid (see Section 2) is generated. Since in this model P_θ we allow for spheroids which are not almost surely bounded, it is not sufficient to simulate the Poisson spheroid process in an enlarged window in order to avoid edge effects, see Chiu et al. (2013, Sect. 3.1.4). Rather we need an exact simulation method. From the two available general approaches given in Lantuéjoul (2002, Sect. 13.2.1) and Lantuéjoul (2013) the one in the latter reference is appropriate but has to be tailored to our specific model. We postpone the details to the Appendix. Then, all spheroids hitting the planar observation window inside the section plane $\mathcal{H}$ are identified and the corresponding intersection ellipses are determined. In the sense of an edge correction only ellipses are considered which have their centre inside the planar observation window. The simulated data then consists of a random number n of triples (C_l, S_l, α_l), $l \in J = \{1, \ldots, n\}$.

For the *unfolding* procedure we consider several grades of fineness for binning the ranges of the 2D data. Since binning the data is a particular case of a kernel density estimation the known problem of small biases and large variances for small bin widths as well as large biases and small variances for large bin widths applies, and the optimal bin width minimizing the mean squared error is unknown. The choices for the numbers (N_C, N_S, N_α) of bins, ordered from coarse to fine binning, are

$$(6, 5, 6), \quad (8, 5, 8), \quad (12, 7, 10), \quad (15, 10, 12), \quad (18, 12, 15). \tag{10}$$

After unfolding the parameters are estimated by maximum likelihood according to the likelihoods given in Section 3.2. These in total five methods are denoted as 'UMLE_1', 'UMLE_2', 'UMLE_3', 'UMLE_4' and 'UMLE_5' in the order of the grade of fineness for the binning as in (10).

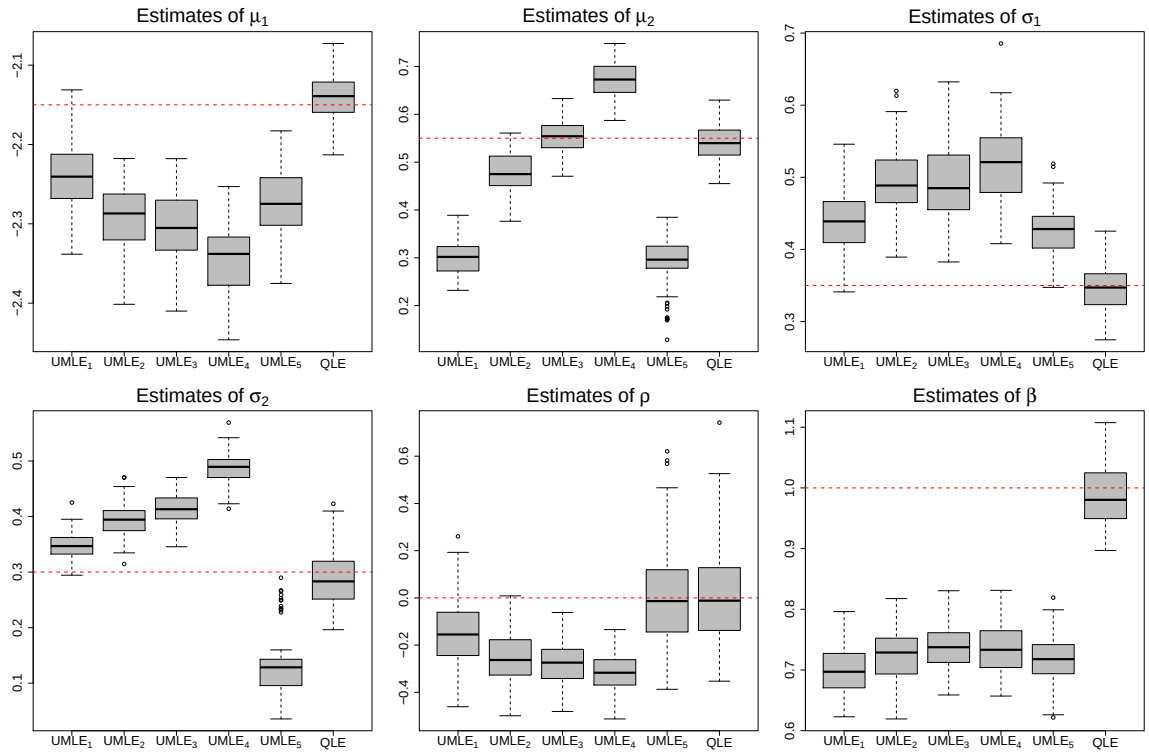

Figure 2: Boxplots of the parameter estimates for original parameters $(\mu_1, \mu_2, \sigma_1, \sigma_2, \varrho, \beta) = (-2.15, 0.55, 0.35, 0.3, 0.0, 1.0)$ (indicated by red dashed lines) from 2D sections with unfolding based on five different bin widths followed each by maximum likelihood estimation (UMLE_1,...,UMLE_5) as well as with quasi-likelihood estimation (QLE).

Furthermore, writing 'med' for the *median*, 'mad' for the *median absolute deviation* and 'cor' for *Pearson's correlation coefficient*, we employ for the *quasi-likelihood estimation*, denoted by 'QLE', the twelve statistics

$$\begin{aligned}
&\mathrm{med}\big(\{\log(C_l)\}_{l\in J}\big),\ \mathrm{med}\big(\{\log(A_l)\}_{l\in J}\big),\ \mathrm{med}\big(\{Y_l\}_{l\in J}\big),\ \mathrm{med}\big(\{S_l\}_{l\in J}\big),\ \mathrm{med}\big(\{\alpha_l\}_{l\in J}\big)\\
&\mathrm{mad}\big(\{\log(C_l)\}_{l\in J}\big),\ \mathrm{mad}\big(\{\log(A_l)\}_{l\in J}\big),\ \mathrm{mad}\big(\{Y_l\}_{l\in J}\big),\ \mathrm{mad}\big(\{S_l\}_{l\in J}\big),\ \mathrm{mad}\big(\{\alpha_l\}_{l\in J}\big)\\
&\mathrm{cor}\big(\{\log(C_l)\}_{l\in J}, \{\log(A_l)\}_{l\in J}\big),\ \mathrm{cor}\big(\{\log(A_l)\}_{l\in J}, \{Y_l\}_{l\in J}\big),
\end{aligned}$$

where $A_l = C_l/S_l$ and $Y_l = \log(S_l/(1-S_l))$, $l \in J$.

In order not only to have a comparison between the six methods applied to the 2D data but to assess somehow the precision of the respective estimates we have considered estimating the parameters from 3D data, that is, for the case that the spheroids were observable directly and not through a planar section. Besides *maximum likelihood estimation* (denoted by 'MLE3D') applied to raw 3D data (c_l, s_l, ϑ_l) we also employ *maximum likelihood estimation* as in Section 3.2 *after binning* the raw data according to the same classification (10) as used for the 2D data, denoting these methods by 'BINMLE_1', 'BINMLE_2', 'BINMLE_3', 'BINMLE_4' and 'BINMLE_5'. Since the latter six methods are based on a different kind of data as the first six methods, each a sub-sample of (the respective 2D sample) size n was taken.

With each 100 repetitions we have considered four different combinations of parameters.

Table 1: Root mean squared error (rmse) of the parameter estimates for original parameters $(\mu_1, \mu_2, \sigma_1, \sigma_2, \varrho, \beta) = (-2.15, 0.55, 0.35, 0.3, 0.0, 1.0)$ (top) from 2D sections with unfolding based on five different bin widths followed each by maximum likelihood estimation (UMLE_1,...,UMLE_5) as well as with quasi-likelihood estimation (QLE), and (bottom) from 3D data with maximum likelihood for the raw data (MLE3D) and with maximum likelihood after classifying the raw data into the same five binnings as used for unfolding (BINMLE_1,...,BINMLE_5).

Method	rmse($\hat{\mu}_1$)	rmse($\hat{\mu}_2$)	rmse($\hat{\sigma}_1$)	rmse($\hat{\sigma}_2$)	rmse($\hat{\varrho}$)	rmse($\hat{\beta}$)
UMLE_1	0.098	0.252	0.100	0.051	0.215	0.302
UMLE_2	0.147	0.082	0.151	0.096	0.277	0.279
UMLE_3	0.162	0.033	0.152	0.117	0.291	0.265
UMLE_4	0.198	0.127	0.176	0.189	0.326	0.267
UMLE_5	0.130	0.261	0.082	0.180	0.218	0.284
QLE	0.030	0.037	0.028	0.050	0.193	0.049

Method	rmse($\hat{\mu}_1$)	rmse($\hat{\mu}_2$)	rmse($\hat{\sigma}_1$)	rmse($\hat{\sigma}_2$)	rmse($\hat{\varrho}$)	rmse($\hat{\beta}$)
BINMLE_1	0.012	0.012	0.010	0.009	0.039	0.031
BINMLE_2	0.011	0.011	0.008	0.009	0.041	0.036
BINMLE_3	0.010	0.009	0.009	0.008	0.037	0.036
BINMLE_4	0.012	0.010	0.009	0.007	0.033	0.034
BINMLE_5	0.014	0.042	0.013	0.087	0.090	0.034
MLE3D	0.011	0.009	0.008	0.006	0.035	0.035

In the first setting the parameters were chosen as

$$\mu_1 = -2.15,\ \mu_2 = 0.55,\ \sigma_1 = 0.35,\ \sigma_2 = 0.3,\ \varrho = 0,\ \beta = 1,$$

that is, with independent size and shape and isotropic orientation distribution. In the second setting all parameters but β are the same, and the choice $\beta = 10$ leads to a relatively strong alignment of the spheroids parallel to a plane. In the third and forth setting all parameters but ϱ are the same as in the first setting, and the choices $\varrho = 0.25$ and $\varrho = 0.75$, respectively, imply two different levels of dependence of size and shape.

The results of the simulation study for the first choice $(-2.15, 0.55, 0.35, 0.3, 0.0, 1.0)$ of parameters, given in Figure 2 in terms of boxplots and in Table 1 in terms of root mean squared errors (corresponding bootstrap standard errors are given in Table 6) show that QLE provides clearly smaller mean squared errors than most of those from UMLE_1,...,UMLE_5, and that the reason for this behaviour is most of all due to the bias resulting from unfolding. The comparison with the maximum likelihood estimates from the 3D data shows that the effect of binning the data into classes is small whatever the grade of fineness is. Likewise the precision of QLE is roughly (only) one order of magnitude worse than that of MLE3D but one order of magnitude better than that of UMLE_1,...,UMLE_5. Figure 2 shows that a particular choice of bins leads for a certain parameter to a precision comparable to that of QLE whereas with the same choice of bins estimation of another parameter implies a certain bias. These findings also hold for other choices of the parameters, see the root mean squared errors in the Tables 2–4 together with the respective bootstrap standard errors in Tables 7–9 (postponed to the Appendix). In particular, it becomes obvious from Table 2 that the error of the estimates

Table 2: Root mean squared error (rmse) of the parameter estimates for original parameters $(\mu_1, \mu_2, \sigma_1, \sigma_2, \varrho, \beta) = (-2.15, 0.55, 0.35, 0.3, 0.0, 10.0)$ (top) from 2D sections with unfolding based on five different bin widths followed each by maximum likelihood estimation (UMLE_1,...,UMLE_5) as well as with quasi-likelihood estimation (QLE), and (bottom) from 3D data with maximum likelihood for the raw data (MLE3D) and with maximum likelihood after classifying the raw data into the same five binnings as used for unfolding (BINMLE_1,...,BINMLE_5).

Method	rmse($\hat{\mu}_1$)	rmse($\hat{\mu}_2$)	rmse($\hat{\sigma}_1$)	rmse($\hat{\sigma}_2$)	rmse($\hat{\varrho}$)	rmse($\hat{\beta}$)
UMLE_1	0.066	0.296	0.098	0.040	0.202	6.405
UMLE_2	0.126	0.043	0.130	0.229	0.315	5.989
UMLE_3	0.139	0.073	0.137	0.269	0.339	5.407
UMLE_4	0.183	0.235	0.163	0.370	0.373	5.149
UMLE_5	0.120	0.257	0.095	0.205	0.237	6.381
QLE	0.034	0.069	0.038	0.049	0.323	0.418

Method	rmse($\hat{\mu}_1$)	rmse($\hat{\mu}_2$)	rmse($\hat{\sigma}_1$)	rmse($\hat{\sigma}_2$)	rmse($\hat{\varrho}$)	rmse($\hat{\beta}$)
BINMLE_1	0.011	0.010	0.010	0.008	0.035	0.730
BINMLE_2	0.012	0.010	0.009	0.007	0.036	0.532
BINMLE_3	0.011	0.009	0.009	0.008	0.035	0.480
BINMLE_4	0.011	0.008	0.008	0.007	0.030	0.436
BINMLE_5	0.014	0.041	0.010	0.085	0.088	0.738
MLE3D	0.010	0.009	0.007	0.007	0.029	0.330

Table 3: Root mean squared error (rmse) of the parameter estimates for original parameters $(\mu_1, \mu_2, \sigma_1, \sigma_2, \varrho, \beta) = (-2.15, 0.55, 0.35, 0.3, 0.25, 1.0)$ from 2D sections with unfolding based on five different bin widths followed each by maximum likelihood estimation (UMLE_1,...,UMLE_5) as well as with quasi-likelihood estimation (QLE).

Method	rmse($\hat{\mu}_1$)	rmse($\hat{\mu}_2$)	rmse($\hat{\sigma}_1$)	rmse($\hat{\sigma}_2$)	rmse($\hat{\varrho}$)	rmse($\hat{\beta}$)
UMLE_1	0.117	0.237	0.090	0.051	0.264	0.297
UMLE_2	0.154	0.075	0.140	0.091	0.400	0.270
UMLE_3	0.174	0.033	0.150	0.109	0.425	0.262
UMLE_4	0.208	0.131	0.173	0.183	0.474	0.265
UMLE_5	0.161	0.231	0.077	0.209	0.200	0.284
QLE	0.035	0.055	0.035	0.040	0.286	0.059

Table 4: Root mean squared error (rmse) of the parameter estimates for original parameters $(\mu_1, \mu_2, \sigma_1, \sigma_2, \varrho, \beta) = (-2.15, 0.55, 0.35, 0.3, 0.75, 1.0)$ from 2D sections with unfolding based on five different bin widths followed each by maximum likelihood estimation (UMLE_1,...,UMLE_5) as well as with quasi-likelihood estimation (QLE).

Method	rmse($\hat{\mu}_1$)	rmse($\hat{\mu}_2$)	rmse($\hat{\sigma}_1$)	rmse($\hat{\sigma}_2$)	rmse($\hat{\varrho}$)	rmse($\hat{\beta}$)
UMLE_1	0.171	0.175	0.099	0.050	0.420	0.302
UMLE_2	0.191	0.041	0.141	0.087	0.678	0.281
UMLE_3	0.213	0.067	0.151	0.103	0.697	0.275
UMLE_4	0.242	0.178	0.179	0.176	0.798	0.275
UMLE_5	0.221	0.196	0.081	0.236	0.256	0.292
QLE	0.026	0.040	0.025	0.043	0.156	0.059

of $\beta = 10$ from UMLE_1,...,UMLE_5 is almost as large as the parameter. However, in either case QLE as well as UMLE_1,...,UMLE_5 produce large errors when estimating the parameter ϱ, which is not the case when using 3D data, see Tables 1 and 2.

6 Application

We consider two kinds of aluminium matrix composites (see Figure 1) reinforced either with alumina particles (Al_2O_3, ca. 15% volume fraction), denoted by AA6061-15p, or with short fibres (Saffil, ca. 20% volume fraction), denoted by AA6061-20s, as in Müller et al. (2015) where experimental investigations most of all on the very high cycle fatigue behaviour are performed and further details may be found. Due to extrusion moulding into a bar the particles in AA6061-15p were aligned nearly parallel to the extrusion direction, whereas before infiltration with aluminium the short fibres in AA6061-20s had been arranged nearly perpendicular to some preferred direction u, but, apart from that, randomly. Therefore, the production process justifies the assumption that the orientation distribution of both types of inclusions is invariant with respect to rotations about some fixed axis.

For both materials the ceramic inclusions are modelled as prolate spheroids since this kind of geometric shape is quite natural for the short fibres (besides cylinders or sphero-cylinders) and sufficiently flexible for the particles. In order to extract the data for the corresponding ellipses from the planar sections the 2D images have been segmented and ellipses have been fitted with the help of an image analyser (Pau et al., 2010). The aim is to estimate the parameters of the supposed spheroid distribution (see Section 2) from the 2D data with the quasi-likelihood approach. For AA6061-15p we use a section plane parallel to the extrusion direction (see Figure 1, left) which corresponds to a vertical uniform random section as needed for unfolding (see Section 3.1). However, in departure from this setting, for AA6061-20s we use a section plane *perpendicular* to the direction u (see Figure 1, right) since it seemed to be more informative than the section plane parallel to u.

In order to estimate the statistics (see Section 5) needed for QLE an edge correction in the sense of minus-sampling (Chiu et al., 2013, p. 254) has been applied. The results of QLE are given in Table 5.

In order to assess the goodness-of-fit of the QLE parameter estimates we generated each 199 samples of a Poisson spheroid system such that the mean number of spheroids hitting the observation window equals the sample size of the data. From the data and from the simulated

Table 5: Parameter estimates.

	$\hat{\mu}_1$	$\hat{\mu}_2$	$\hat{\sigma}_1$	$\hat{\sigma}_2$	$\hat{\varrho}$	$\hat{\beta}$
AA6061-15p	-3.71	-0.76	0.37	0.66	-0.37	0.18
AA6061-20s	-3.34	-1.98	0.16	0.25	-0.57	3.27

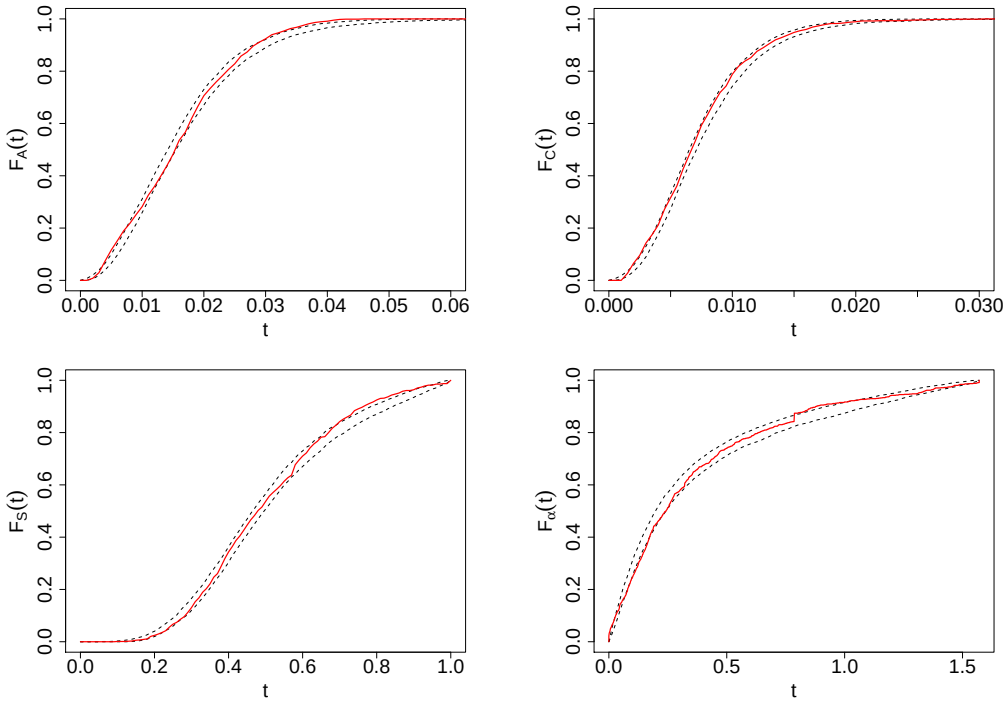

Figure 3: Empirical c.d.f. for the AA6061-15p data (red) and pointwise 95% envelopes of the c.d.f. for the fitted model (black dashed) of length A of the semi-major axis (F_A, top left), of length C of the semi-minor axis (F_C, top right), of shape factor S (F_S, bottom left) and of angle α (F_α, bottom right).

samples each the empirical c.d.f. of the length A of the semi-major axis, of the length C of the semi-minor axis, of the shape factor S and of the direction angle α of the intersection ellipses were determined. In Figures 3 and 4 each the pointwise 95% envelopes of the empirical c.d.f.s from the simulated samples as well as the corresponding empirical c.d.f. of the data are plotted. The small jumps in Figure 3 (bottom right) and in Figure 4 (bottom right) in the empirical c.d.f. F_α w.r.t. to the angle α at 0, $\pi/4$ and $\pi/2$ are clearly due to digitisation. All in all it seems that the fit of the spheroid distribution for AA6061-15p can be considered as satisfying whereas the goodness-of-fit for AA6061-20s is much worse. In particular, for AA6061-20s the employed model seems not to be able to capture the tail behaviour of the lengths A and C of the semi-major and the semi-minor axes.

7 Conclusions

We have demonstrated the potential of the quasi-likelihood estimation approach for inferring the parameters of a distribution of three-dimensional objects which are observable only through

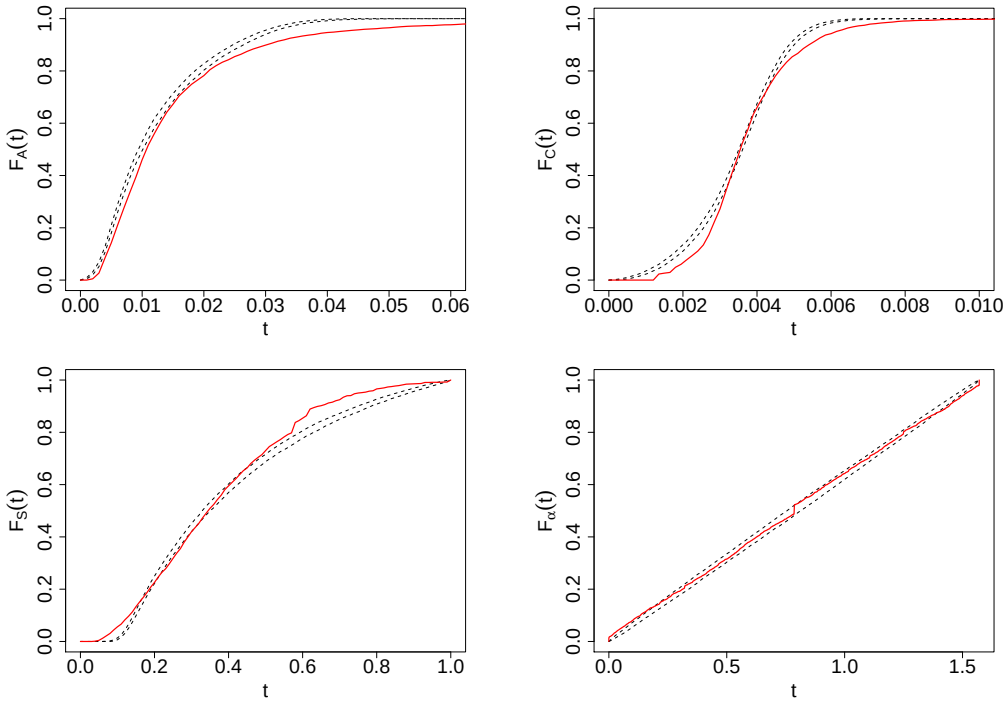

Figure 4: Empirical c.d.f. for the AA6061-20s data (red) and pointwise 95% envelopes of the c.d.f. for the fitted model (black dashed) of length A of the semi-major axis (F_A, top left), of length C of the semi-minor axis (F_C, top right), of shape factor S (F_S, bottom left) and of angle α (F_α, bottom right).

two-dimensional sections, even in the more complicated situation that objective functions are only available as Monte Carlo approximations. Although for certain bin widths of the histograms the precision of the parameter estimates with the maximum likelihood method after the well-known procedure of unfolding is comparable to the precision of the quasi-likelihood estimates the respective bin widths are not known in advance and, more seriously, in general differ for the different parameters. At least in the case of a *parametric* modelling approach the quasi-likelihood estimation approach should thus be considered as a valuable alternative. For a *non-parametric* modelling approach, however, unfolding will keep indispensable.

Although the employed parametric model for the random prolate spheroids is of course a particular one, the two investigated methods of parameter estimation might be easily adapted to other models. We would then expect a similar behaviour w.r.t. the precision of the parameter estimates.

For the two real-world samples it turns out that the particular parametric model is able to model the distribution of the ceramic particles in AA6061-15p reasonable well whereas for the distribution of the ceramic short fibres in AA6061-20s the model can only be used as a rough approximation since the tail behaviour is not reflected appropriately.

Acknowledgments

Support of the research by the German Research Foundation (DFG) within the priority programme "Life$^\infty$" (SPP 1466) is gratefully acknowledged.

A Exact simulation

Since for a prolate spheroid the length of the semi-major axis equals the radius of the smallest circumscribed ball the distribution of this radius is directly given which makes the following exact simulation method quite efficient.

Denoting by $B(x,r)$ a ball in $\mathbb{R}^3$ with centre $x \in \mathbb{R}^3$ and radius $r \in [0,\infty)$ let $[W] = \{(x,r) \in \mathbb{R}^3 \times [0,\infty) : B(x,r) \cap W \neq \varnothing\}$ for some convex compact set $W \subset \mathbb{R}^3$. Let Ψ be a marked point process on $\mathbb{R}^3 \times [0,\infty)$ representing a stationary Poisson ball process (Schneider and Weil, 2008, Sect. 4.1) with intensity λ and p.d.f. f_R (with finite third moment) of the balls' radii. Then the mean number of balls from Ψ hitting W equals

$$\begin{aligned}\Lambda_\Psi([W]) &= \int_{\mathbb{R}^3}\int_0^\infty \lambda\, f_R(r)\, \mathbf{1}_{[W]}(x,r)\,\mathrm{d}r\,\mathrm{d}x = \int_{\mathbb{R}^3}\int_0^\infty \lambda\, f_R(r)\, \mathbf{1}_{W\oplus B(o,r)}(x)\,\mathrm{d}r\,\mathrm{d}x \\ &= \int_0^\infty \lambda\, f_R(r)\, V(W\oplus B(o,r))\,\mathrm{d}r = \int_0^\infty \lambda\, f_R(r) \sum_{k=0}^3 a_k r^k\,\mathrm{d}r = \lambda \sum_{k=0}^3 a_k \mathsf{E}(R^k),\end{aligned}$$

where $W \oplus B(o,r) = \{x+y : x \in W, y \in B(o,r)\}$ and R denotes the random ball radius, and where we have used first Fubini's theorem and then Steiner's formula; the latter implying $a_0 = V(W)$, $a_1 = S(W)$ (the surface area of W), $a_2 = M(W)$ (the integral of mean curvature of W) and $a_3 = 4\pi/3$, see Chiu et al. (2013, p. 15f.) and Schneider and Weil (2008, p. 600ff.).

Hence, $\Psi([W])$ follows a Poisson distribution with mean $\lambda \sum_{k=0}^3 a_k \mathsf{E}(R^k)$. Given $\Psi([W]) = n$ the n points $(x_1,r_1),\ldots,(x_n,r_n)$ from Ψ are i.i.d. according to $\Lambda_\Psi(\cdot)/\Lambda_\Psi([W])$, i. e. with joint p.d.f.

$$f^{[W]}(x,r) = \frac{\lambda\, f_R(r)\, \mathbf{1}_{W\oplus B(o,r)}(x)}{\Lambda_\Psi([W])},$$

see also Lantuéjoul (2002, Prop. 13.2.1) and Lantuéjoul (2013). This implies that the radii $r_1,\ldots,r_n$ are distributed according to the p.d.f.

$$f^{[W]}(r) = \int_{\mathbb{R}^3} f^{[W]}(x,r)\,\mathrm{d}x = \frac{\lambda\, f_R(r)\, V(W\oplus B(o,r))}{\Lambda_\Psi([W])} = \sum_{k=0}^3 \frac{a_k r^k f_R(r)}{\sum_{j=0}^3 a_j \mathsf{E}(R^j)}$$

and, given the radius r, the centre x is uniformly distributed on $W \oplus B(o,r)$,

$$f^{[W]}(x|r) = \frac{f^{[W]}(x,r)}{f^{[W]}(r)} = \frac{\mathbf{1}_{W\oplus B(o,r)}(x)}{V(W\oplus B(o,r))}.$$

Hence, for the exact simulation of a stationary Poisson ball process w.r.t. the window W, the following algorithm (Algorithm 1 in Lantuéjoul, 2013) is suitable:

Algorithm 1.

1. Generate n according to the Poisson distribution with mean $\Lambda_\Psi([W])$.

2. Generate $r_1, \ldots, r_n$ i.i.d. according to $f^{[W]}(r)$.

3. Generate $x_1, \ldots, x_n$ independently and, each conditionally on r_i, uniformly on $W \oplus B(o, r_i)$, $i = 1, \ldots, n$.

In the most crucial step 2 in algorithm 1 the distribution is a mixture, i. e. in terms of the respective c.d.f. $F^{[W]}(r)$ we have

$$F^{[W]}(r) = \sum_{k=0}^{3} \frac{a_k \mathsf{E}(R^k; R \le r)}{\sum_{j=0}^{3} a_j \mathsf{E}(R^j)} = \sum_{k=0}^{3} \frac{a_k \mathsf{E}(R^k)}{\sum_{j=0}^{3} a_j \mathsf{E}(R^j)} \frac{\mathsf{E}(R^k; R \le r)}{\mathsf{E}(R^k)}$$

with weights

$$p_k = \frac{a_k \mathsf{E}(R^k)}{\sum_{j=0}^{3} a_j \mathsf{E}(R^j)}.$$

Since the random ball radius R has a log-normal distribution $\mathsf{logN}(\mu, \sigma^2)$, i. e.

$$f_R(r) = \frac{1}{\sqrt{2\pi}\sigma\, r} \exp\left(-\frac{(\log(r) - \mu)^2}{2\sigma^2}\right),$$

where $\mu \in \mathbb{R}$ and $\sigma > 0$, we have – as a somewhat nice fact – that for all $k = 0, 1, \ldots$

$$\frac{\mathsf{E}(R^k; R \le r)}{\mathsf{E}(R^k)} = \Phi\left(\frac{\log(r) - (\mu + k\sigma^2)}{\sigma}\right)$$

(with Φ the c.d.f. of a standard normal distribution) is the c.d.f. of a log-normal distribution $\mathsf{logN}(\mu + k\sigma^2, \sigma^2)$. Likewise we have $\mathsf{E}(R^k) = \exp(k\mu + k^2\sigma^2/2)$, $k = 0, 1, 2, 3$. Hence, in order to generate random numbers according to $f^{[W]}(r)$ we can apply the following algorithm (similar to Algorithm 2 in Lantuéjoul, 2013):

Algorithm 2.

1. Generate a random integer k from $\{0, 1, 2, 3\}$ according to the probabilities

$$p_k = \frac{a_k \exp(k\mu + k^2\sigma^2/2)}{\sum_{j=0}^{3} a_j \exp(j\mu + j^2\sigma^2/2)}.$$

2. Deliver a random number from a $\mathsf{logN}(\mu + k\sigma^2, \sigma^2)$-distribution.

Once all circumscribed balls hitting W are generated subsequently the shapes and orientations (see B) of the prolate spheroids can be generated. In case one is interested only in a configuration of spheroids hitting W then possibly a few non-hitting spheroids have to be deleted from the configuration as the final step.

B Simulation of orientations

From (1) we have

$$h_\beta(\vartheta) = \frac{1}{2} \frac{\beta \sin\vartheta}{(1 + (\beta^2 - 1)\cos^2\vartheta)^{\frac{3}{2}}}, \quad \vartheta \in [0, \pi), \tag{11}$$

Table 6: Bootstrap standard errors of the estimated root mean squared errors in Table 1.

Method	rmse($\hat{\mu}_1$)	rmse($\hat{\mu}_2$)	rmse($\hat{\sigma}_1$)	rmse($\hat{\sigma}_2$)	rmse($\hat{\varrho}$)	rmse($\hat{\beta}$)
UMLE_1	0.004	0.004	0.004	0.002	0.012	0.004
UMLE_2	0.004	0.005	0.004	0.003	0.010	0.004
UMLE_3	0.004	0.005	0.002	0.003	0.009	0.003
UMLE_4	0.004	0.005	0.003	0.003	0.008	0.004
UMLE_5	0.004	0.003	0.005	0.005	0.017	0.004
QLE	0.002	0.002	0.002	0.003	0.017	0.003
BINMLE_1	0.001	0.001	0.001	0.001	0.002	0.002
BINMLE_2	0.001	0.001	0.001	0.001	0.003	0.002
BINMLE_3	0.001	0.001	0.001	0.000	0.002	0.002
BINMLE_4	0.001	0.001	0.001	0.000	0.002	0.002
BINMLE_5	0.001	0.001	0.003	0.008	0.007	0.003
MLE3D	0.001	0.001	0.001	0.000	0.002	0.002

Table 7: Bootstrap standard errors of the estimated root mean squared errors in Table 2.

Method	rmse($\hat{\mu}_1$)	rmse($\hat{\mu}_2$)	rmse($\hat{\sigma}_1$)	rmse($\hat{\sigma}_2$)	rmse($\hat{\varrho}$)	rmse($\hat{\beta}$)
UMLE_1	0.003	0.004	0.003	0.002	0.012	0.018
ULME_2	0.004	0.005	0.003	0.002	0.009	0.017
ULME_3	0.004	0.005	0.004	0.003	0.009	0.022
ULME_4	0.004	0.005	0.004	0.002	0.008	0.023
ULME_5	0.003	0.003	0.007	0.004	0.016	0.018
QLE	0.002	0.002	0.005	0.003	0.025	0.026
BINMLE_1	0.001	0.001	0.001	0.001	0.002	0.059
BINMLE_2	0.001	0.001	0.001	0.000	0.003	0.044
BINMLE_3	0.001	0.001	0.001	0.000	0.002	0.033
BINMLE_4	0.001	0.001	0.001	0.000	0.002	0.036
BINMLE_5	0.001	0.001	0.003	0.008	0.006	0.056
MLE3D	0.001	0.000	0.001	0.000	0.002	0.023

and

$$H_\beta(\vartheta) = \frac{1}{2}\left(1 - \frac{\beta\cos\vartheta}{(1+(\beta^2-1)\cos^2\vartheta)^{\frac{1}{2}}}\right), \quad \vartheta \in [0,\pi), \tag{12}$$

for, respectively, the p.d.f. and the c.d.f. of the polar angle ϑ. This in turn leads to the quantile function

$$H_\beta^{-1}(q) = \arccos\left(\frac{1-2q}{\sqrt{\beta^2-(1-2q)^2(\beta^2-1)}}\right) \tag{13}$$

which can be used to generate random numbers according to H_β with the inversion method.

C Bootstrap standard errors

In Tables 6–9 the bootstrap standard errors of the estimated root mean squared errors given in Tables 1–4 are provided.

Table 8: Bootstrap standard errors of the estimated root mean squared errors in Table 3.

Method	rmse($\hat{\mu}_1$)	rmse($\hat{\mu}_2$)	rmse($\hat{\sigma}_1$)	rmse($\hat{\sigma}_2$)	rmse($\hat{\varrho}$)	rmse($\hat{\beta}$)
UMLE_1	0.004	0.004	0.004	0.002	0.015	0.004
ULME_2	0.004	0.004	0.003	0.002	0.011	0.004
ULME_3	0.004	0.004	0.002	0.002	0.009	0.003
ULME_4	0.004	0.005	0.003	0.003	0.008	0.004
ULME_5	0.004	0.003	0.006	0.004	0.014	0.004
QLE	0.003	0.003	0.003	0.003	0.021	0.004

Table 9: Bootstrap standard errors of the estimated root mean squared errors in Table 4.

Method	rmse($\hat{\mu}_1$)	rmse($\hat{\mu}_2$)	rmse($\hat{\sigma}_1$)	rmse($\hat{\sigma}_2$)	rmse($\hat{\varrho}$)	rmse($\hat{\beta}$)
UMLE_1	0.004	0.003	0.005	0.002	0.015	0.005
ULME_2	0.004	0.004	0.003	0.003	0.012	0.004
ULME_3	0.004	0.004	0.003	0.002	0.012	0.004
ULME_4	0.004	0.005	0.003	0.002	0.011	0.004
ULME_5	0.008	0.004	0.007	0.004	0.015	0.004
QLE	0.002	0.002	0.003	0.003	0.014	0.004

References

M. Baaske. unfoldr: Stereological Unfolding for Spheroidal Particles. R package version 0.5.8, http://cran.r-project.org/package=unfoldr, 2016a.

M. Baaske. QLE. R package version 0.1, http://cran.r-project.org/package=QLE, 2016b.

M. Baaske, F. Ballani, and K. G. van den Boogaart. A quasi-likelihood approach to parameter estimation for simulatable statistical models. *Image Anal. Stereol.*, 33:107–119, 2014.

V. Beneš and P. Krejčíř. Decomposition in stereological unfolding problems. *Kybernetika*, 33: 245–258, 1997.

V. Beneš and J. Rataj. *Stochastic Geometry: Selected Topics*. Kluwer, Boston, 2004.

V. Beneš, M. Jiruše, and M. Slámová. Stereological unfolding of the trivariate size-shape-orientation distribution of spheroidal particles with application. *Acta Materialia*, 45:1105–1113, 1997.

S. N. Chiu, D. Stoyan, W. S. Kendall, and J. Mecke. *Stochastic Geometry and its Applications*. J. Wiley & Sons, Chichester, 3rd edition, 2013.

L. M. Cruz-Orive. Particle size-shape distributions: the general spheroid problem. *J. Microscopy*, 107:235–253, 1976.

J. Franke, C. Redenbach, and N. Zhang. On a mixture model for directional data on the sphere. *Scand. J. Statist.*, 43(1):139–155, 2016.

C. C. Heyde. *Quasi-Likelihood and Its Applications: A General Approach to Optimal Parameter Estimation*. Springer, New York, 1997.

C. Lantuéjoul. *Geostatistical Simulation.* Springer, Berlin, 2002.

C. Lantuéjoul. Exact simulation of a Boolean model. *Image Anal. Stereol.*, 32:101–105, 2013.

A. Müller, A. Weidner, and H. Biermann. Influence of reinforcement geometry on the very high-cycle fatigue behavior of aluminum-matrix-composites. *Materials Science Forum*, 825/826:150–157, 2015.

W. Nagel. Stereology. In I. Molchanov W. S. Kendall, editor, *New perspectives in stochastic geometry*, pages 451–475. Oxford University Press, Oxford, 2010.

J. Ohser and F. Mücklich. *Statistical Analysis of Microstructures in Materials Science.* J. Wiley & Sons, Chichester, 2000.

J. Ohser and K. Schladitz. *3D Images of Material Structures.* Wiley-VCH, Weinheim, 2009.

M. R. Osborne. Fisher's method of scoring. *Int. Stat. Rev.*, 60:99–117, 1992.

G. Pau, F. Fuchs, O. Sklyar, M. Boutros, and W. Huber. Ebimage Ű an r package for image processing with applications to cellular phenotypes. *Bioinformatics*, 26(7):979–981, 2010.

R. Schneider and W. Weil. *Stochastic and Integral Geometry.* Springer, Berlin, 2008.

S. D. Wicksell. The corpuscle problem. II: Case of ellipsoidal corpuscles. *Biometrika*, 18: 151–172, 1926.